Linear antenna microwave chemical vapour deposition of diamond films on long-period fiber gratings for bio-sensing applications

M. Ficek,[1,2] P. Niedziałkowski,[3] M. Śmietana,[4] M. Koba,[4] S. Drijkoningen,[2,5] R. Bogdanowicz,[1] W. J. Bock,[6] and K. Haenen[2,5]

[1]*Department of Metrology and Optoelectronics, Faculty of Electronics, Telecommunications and Informatics, Gdansk University of Technology, 11/12 G. Narutowicza St., 80-233 Gdansk, Poland*

[2]*Institute for Materials Research (IMO), Hasselt University, Wetenschapspark 1, B-3590 Diepenbeek, Belgium*

[3]*Department of Analytical Chemistry, Faculty of Chemistry, University of Gdansk, 63 Wita Stwosza St., 80-952 Gdansk, Poland*

[4]*Institute of Microelectronics and Optoelectronics, Warsaw University of Technology, Koszykowa 75, 00-662 Warszawa, Poland*

[5]*IMOMEC, IMEC vzw, Wetenschapspark 1, B-3590 Diepenbeek, Belgium*

[6]*Centre de Recherche en Photonique, Université du Québec en Outaouais, 101 Rue Saint-Jean-Bosco, Gatineau, QC J8X 3X7, Canada*

Abstract. The growth processes of nanocrystalline diamond (NCD) thin films on fused silica optical fibers with UV-induced long-period gratings (LPGs) were investigated with regard to biosensing applications. The films were deposited using a linear antenna microwave plasma enhanced chemical vapor deposition system, which allows for the growth of diamond at temperatures below 350°C. The films exhibited a high refractive index n = 2.32, as estimated at λ = 550 nm. The biosensing applications of NCD-coated LPG were considered in relation to bovine serum albumin (BSA) as an external medium. In response to BSA binding and the subsequent formation of a thin bio-layer on the NCD surface, the LPG resonances slightly split and shifted towards lower wavelengths.

OCIS codes: (310.0310) Thin films; (160.0160) Materials; (060.2370) Fiber optics sensors.

References and links

1. S. Yin, P. B. Ruffin, and F. T. S. Yu, *Fiber Optic Sensors, Second Edition* (CRC Press, 2008).
2. M. Jędrzejewska-Szczerska, P. Wierzba, A. A. Chaaya, M. Bechelany, P. Miele, R. Viter, A. Mazikowski, K. Karpienko, and M. Wróbel, "ALD thin ZnO layer as an active medium in a fiber-optic Fabry–Perot interferometer," Sens. Actuators Phys. **221**, 88–94 (2015).
3. L. S. Grattan and B. T. Meggitt, *Optical Fiber Sensor Technology: Chemical and Environmental Sensing* (Springer Science & Business Media, 2013).
4. A. M. Vengsarkar, P. J. Lemaire, J. B. Judkins, V. Bhatia, T. Erdogan, and J. E. Sipe, "Long-period fiber gratings as band-rejection filters," J. Lightwave Technol. **14**(1), 58–65 (1996).
5. X. Shu, L. Zhang, and I. Bennion, "Sensitivity Characteristics of Long-Period Fiber Gratings," J. Lightwave Technol. **20**(2), 255–266 (2002).
6. V. Bhatia, D. Campbell, R. O. Claus, and A. M. Vengsarkar, "Simultaneous strain and temperature measurement with long-period gratings," Opt. Lett. **22**(9), 648–650 (1997).
7. R. Bogdanowicz, M. Sobaszek, J. Ryl, M. Gnyba, M. Ficek, Ł. Gołuński, W. J. Bock, M. Śmietana, and K. Darowicki, "Improved surface coverage of an optical fibre with nanocrystalline diamond by the application of dip-coating seeding," Diamond Related Materials **55**, 52–63 (2015).
8. H. S. Jang, K. N. Park, J. P. Kim, S. J. Sim, O. J. Kwon, Y.-G. Han, and K. S. Lee, "Sensitive DNA biosensor based on a long-period grating formed on the side-polished fiber surface," Opt. Express **17**(5), 3855–3860 (2009).
9. M. Janczuk-Richter, M. Dominik, E. Roźniecka, M. Koba, P. Mikulic, W. J. Bock, M. Łoś, M. Śmietana, and J. Niedziółka-Jönsson, "Long-period fiber grating sensor for detection of viruses," Sens. Actuators B Chem. **250**, 32–38 (2017).

10. M. Sobaszek, Ł. Skowroński, R. Bogdanowicz, K. Siuzdak, A. Cirocka, P. Zięba, M. Gnyba, M. Naparty, Ł. Gołuński, and P. Płotka, "Optical and electrical properties of ultrathin transparent nanocrystalline boron-doped diamond electrodes," Opt. Mater. **42**, 24–34 (2015).
11. M. Wąsowicz, M. Ficek, M. S. Wróbel, R. Chakraborty, D. Fixler, P. Wierzba, and M. Jędrzejewska-Szczerska, "Haemocompatibility of Modified Nanodiamonds," Materials (Basel) **10**(4), 352 (2017).
12. M. Amaral, A. G. Dias, P. S. Gomes, M. A. Lopes, R. F. Silva, J. D. Santos, and M. H. Fernandes, "Nanocrystalline diamond: In vitro biocompatibility assessment by MG63 and human bone marrow cells cultures," J. Biomed. Mater. Res. A **87**(1), 91–99 (2008).
13. R. Bogdanowicz, M. Śmietana, M. Gnyba, Ł. Gołunski, J. Ryl, and M. Gardas, "Optical and structural properties of polycrystalline CVD diamond films grown on fused silica optical fibres pre-treated by high-power sonication seeding," Appl. Phys., A Mater. Sci. Process. **116**(4), 1927–1937 (2014).
14. R. Bogdanowicz, M. Śmietana, M. Gnyba, M. Ficek, V. Straňák, Ł. Goluński, M. Sobaszek, and J. Ryl, "Nucleation and growth of CVD diamond on fused silica optical fibres with titanium dioxide interlayer," Phys. Status Solidi., A Appl. Mater. Sci. **210**(10), 1991–1997 (2013).
15. E. Scorsone, S. Saada, J. C. Arnault, and P. Bergonzo, "Enhanced control of diamond nanoparticle seeding using a polymer matrix," J. Appl. Phys. **106**(1), 014908 (2009).
16. M. Ficek, R. Bogdanowicz, and J. Ryl, "Nanocrystalline CVD Diamond Coatings on Fused Silica Optical Fibres: Optical Properties Study," Acta Phys Pol Ser A **127**(3), 868–873 (2015).
17. Š. Potocký, O. Babchenko, K. Hruška, and A. Kromka, "Linear antenna microwave plasma CVD diamond deposition at the edge of no-growth region of C−H−O ternary diagram," Phys. Status Solidi, B Basic Res. **249**(12), 2612–2615 (2012).
18. A. Kromka, O. Babchenko, T. Izak, K. Hruska, and B. Rezek, "Linear antenna microwave plasma CVD deposition of diamond films over large areas," Vacuum **86**(6), 776–779 (2012).
19. M. Varga, Z. Remes, O. Babchenko, and A. Kromka, "Optical study of defects in nano-diamond films grown in linear antenna microwave plasma CVD from H2/CH4/CO2 gas mixture," Phys. Status Solidi, B Basic Res. **249**(12), 2635–2639 (2012).
20. M. Ficek, M. Sobaszek, M. Gnyba, J. Ryl, Ł. Gołuński, M. Smietana, J. Jasiński, P. Caban, and R. Bogdanowicz, "Optical and electrical properties of boron doped diamond thin conductive films deposited on fused silica glass substrates," Appl. Surf. Sci. **387**, 846–856 (2016).
21. M. Ficek, S. Drijkoningen, J. Karczewski, R. Bogdanowicz, and K. Haenen, "Low temperature growth of diamond films on optical fibers using Linear Antenna CVD system," IOP Conf. Ser. Mater. Sci. Eng. **104**, 012025 (2016).
22. M. Smietana, W. J. Bock, P. Mikulic, and J. Chen, "Increasing sensitivity of arc-induced long-period gratings—pushing the fabrication technique toward its limits," Meas. Sci. Technol. **22**(1), 015201 (2011).
23. A. Taylor, F. Fendrych, L. Fekete, J. Vlček, V. Řezáčová, V. Petrák, J. Krucký, M. Nesládek, and M. Liehr, "Novel high frequency pulsed MW-linear antenna plasma-chemistry: Routes towards large area, low pressure nanodiamond growth," Diamond Related Materials **20**(4), 613–615 (2011).
24. M. Liehr, F. Fendrych, A. Taylor, and M. Nesládek, "Routes towards large area, low pressure nanodiamond growth via pulsed microwave linear antenna plasma chemistry," MRS Proc. **1282** (1282:mrsf10-1282-a03-01) (2011).
25. O. A. Chaves, V. A. da Silva, C. M. R. Sant'Anna, A. B. B. Ferreira, T. A. N. Ribeiro, M. G. de Carvalho, D. Cesarin-Sobrinho, and J. C. Netto-Ferreira, "Binding studies of lophirone B with bovine serum albumin (BSA): Combination of spectroscopic and molecular docking techniques," J. Mol. Struct. **1128**, 606–611 (2017).
26. N. El Kadi, N. Taulier, J. Y. Le Huérou, M. Gindre, W. Urbach, I. Nwigwe, P. C. Kahn, and M. Waks, "Unfolding and Refolding of Bovine Serum Albumin at Acid pH: Ultrasound and Structural Studies," Biophys. J. **91**(9), 3397–3404 (2006).
27. M. Ficek, K. J. Sankaran, J. Ryl, R. Bogdanowicz, I.-N. Lin, K. Haenen, and K. Darowicki, "Ellipsometric investigation of nitrogen doped diamond thin films grown in microwave CH4/H2/N2 plasma enhanced chemical vapor deposition," Appl. Phys. Lett. **108**(24), 241906 (2016).
28. H. Tompkins and E. A. Irene, *Handbook of Ellipsometry* (William Andrew, 2005).
29. S. Drijkoningen, P. Pobedinskas, S. Korneychuk, A. Momot, Y. Balasubramaniam, M. K. Van Bael, S. Turner, J. Verbeeck, M. Nesládek, and K. Haenen, "On the Origin of Diamond Plates Deposited at Low Temperature," Cryst. Growth Des. **17**(8), 4306–4314 (2017).
30. A. C. Ferrari and J. Robertson, "Origin of the 1150 - cm^{-1} Raman mode in nanocrystalline diamond," Phys. Rev. B **63**(12), 121405 (2001).
31. S. Prawer, K. W. Nugent, D. N. Jamieson, J. O. Orwa, L. A. Bursill, and J. L. Peng, "The Raman spectrum of nanocrystalline diamond," Chem. Phys. Lett. **332**(1-2), 93–97 (2000).
32. S. Logothetidis, M. Gioti, P. Patsalas, and C. Charitidis, "Insights on the deposition mechanism of sputtered amorphous carbon films," Carbon **37**(5), 765–769 (1999).
33. M. Gioti, D. Papadimitriou, and S. Logothetidis, "Optical properties and new vibrational modes in carbon films," Diamond Related Materials **9**(3-6), 741–745 (2000).
34. G. E. Jellison, Jr., V. I. Merkulov, A. A. Puretzky, D. B. Geohegan, G. Eres, D. H. Lowndes, and J. B. Caughman, "Characterization of thin-film amorphous semiconductors using spectroscopic ellipsometry," Thin Solid Films **377–378**, 68–73 (2000).

35. Z. G. Hu and P. Hess, "Optical constants and thermo-optic coefficients of nanocrystalline diamond films at 30–500°C," Appl. Phys. Lett. **89**(8), 081906 (2006).
36. S. Gupta, A. Dudipala, O. A. Williams, K. Haenen, and E. Bohannan, "Ex situ variable angle spectroscopic ellipsometry studies on chemical vapor deposited boron-doped diamond films: Layered structure and modeling aspects," J. Appl. Phys. **104**(7), 073514 (2008).
37. A. Taylor, P. Ashcheulov, M. Čada, L. Fekete, P. Hubík, L. Klimša, J. Olejníček, Z. Remeš, I. Jirka, P. Janíček, E. Bedel-Pereira, J. Kopeček, J. Mistrík, and V. Mortet, "Effect of plasma composition on nanocrystalline diamond layers deposited by a microwave linear antenna plasma-enhanced chemical vapour deposition system," Phys. Status Solidi., A Appl. Mater. Sci. **212**(11), 2418–2423 (2015).
38. O. A. Williams and M. Nesládek, "Growth and properties of nanocrystalline diamond films," Phys. Status Solidi., A Appl. Mater. Sci. **203**(13), 3375–3386 (2006).
39. M. Smietana, J. Szmidt, M. Dudek, and P. Niedzielski, "Optical properties of diamond-like cladding for optical fibres," Diamond Related Materials **13**(4-8), 954–957 (2004).
40. M. Smietana, W. J. Bock, and P. Mikulic, "Temperature sensitivity of silicon nitride nanocoated long-period gratings working in various surrounding media," Meas. Sci. Technol. **22**(11), 115203 (2011).
41. M. Smietana, M. Koba, E. Brzozowska, K. Krogulski, J. Nakonieczny, L. Wachnicki, P. Mikulic, M. Godlewski, and W. J. Bock, "Label-free sensitivity of long-period gratings enhanced by atomic layer deposited TiO_2 nano-overlays," Opt. Express **23**(7), 8441–8453 (2015).
42. M. Śmietana, M. Koba, P. Mikulic, R. Bogdanowicz, and W. J. Bock, "Improved diamond-like carbon coating deposition uniformity on cylindrical sample by its suspension in RF PECVD chamber," Phys. Status Solidi., A Appl. Mater. Sci. **212**(11), 2496–2500 (2015).
43. F. Vollmer, D. Braun, A. Libchaber, M. Khoshsima, I. Teraoka, and S. Arnold, "Protein detection by optical shift of a resonant microcavity," Appl. Phys. Lett. **80**(21), 4057–4059 (2002).
44. R. Slavík, J. Homola, and E. Brynda, "A miniature fiber optic surface plasmon resonance sensor for fast detection of Staphylococcal enterotoxin B," Biosens. Bioelectron. **17**(6-7), 591–595 (2002).
45. M. Sanders, Y. Lin, J. Wei, T. Bono, and R. G. Lindquist, "An enhanced LSPR fiber-optic nanoprobe for ultrasensitive detection of protein biomarkers," Biosens. Bioelectron. **61**, 95–101 (2014).
46. S. Siddhanta, M. S. Wróbel, and I. Barman, "Integration of protein tethering in a rapid and label-free SERS screening platform for drugs of abuse," Chem. Commun. (Camb.) **52**(58), 9016–9019 (2016).

1. Introduction

Optical fibers have been used extensively to develop a number of sensing devices [1], because they facilitate the measurement of various physical quantities such as temperature [2], humidity [3] or pressure [1]. The attractiveness of optical fiber sensors over conventional sensing devices lies in their immunity to electromagnetic interference, chemical inertness, the possibility of remote sensing, and small size. These features make the fiber-optic sensors an ideal platform for monitoring the chemical and biological parameters in harsh environmental conditions or at distant locations. Recently, considerable attention has been focused on the application of optical fiber gratings. Long-period gratings (LPGs) are fiber devices based on the periodical modulation of the refractive index of the fiber core [4]. Under special phase-matching conditions, the grating will couple the fundamental core mode to discrete cladding modes that are rapidly attenuated due to absorption and scattering. This coupling is seen in LPG transmission spectra as a series of resonances whose spectral position depends on both fabrication as well as external conditions. Due to many advantages, which include the simplicity of fabrication, low insertion loss, no back reflection, and small sizes, LPGs have become popular with regard to their application in fiber-optic communication systems and sensing devices [5]. A number of sensors based on LPGs have been proposed for temperature, strain [6], pressure and refractive index (RI) sensing [7]. The main advantage of LPG-based sensors is their high sensitivity to variations in thickness and optical properties of the material surrounding the LPG [8,9].

Optical fibers are typically covered with polymer coatings which protect the fiber against mechanical damage and aging. There is a need for overlay materials that can serve both as sensing and as protecting layer for optical fiber sensors. Such a layer must be sensitive, i.e. reversely change its volume or surface properties under the influence of a selected physical quantity, and it must have a good adhesion to the optical fiber. Diamond is a material with wide range of extraordinary properties [10], i.e. transparent over a broad spectrum region, highly chemically and abrasively resistant, nontoxic and biocompatible. Therefore diamond films are often used as protective coatings in different applications [11]. On the other hand,

the adhesion of diamond to various substrates (in particular glass or metals), or damage of substrates during chemical vapor deposition (CVD) are the factors that limit its wider commercial use [12].

In our previous works, high power sonication seeding was applied to different suspensions (water/DMSO) in order to obtain diamond films on optical fibers [13]. We have observed that high power seeding can induce the erosion/cavitation of optical fibers. In the study on the use of titanium dioxide interlayer, we were able to demonstrate that a ~20 nm thick interlayer enhances the growth of NCD on fused silica substrates [14]. Moreover, dip-coating seeding seems to be a promising method for the efficient seeding of optical fibers because it allows for the easy treatment of long fiber sections. Scorsone et al. proposed seeding in a solution of polyvinyl alcohol (PVA) and detonation nanodiamond (DND) particles [15]. In the present work, PVA was used due to its ability to form thin films as well as its high viscosity and high solubility in water and surfactants [16].

The linear antenna microwave plasma enhanced chemical vapor deposition (LA MW CVD) technology has recently been developed for the growth of NCD layers [17–19]. In such systems, the deposition of high quality diamond at lower temperatures and also on larger areas are more feasible than in ordinary systems [18]. The substrate temperature has a crucial effect on diamond synthesis and the kinetics of pyrolysis reaction on the growth surface [20]. The main advantage of LA MW CVD is the fact that it enables the growth of diamond layers at low temperatures. Diamond films were successfully grown on optical fibers at temperatures less than 350°C, providing a clear improvement of the results presented in our earlier reports [7,21].

In this work, we applied a low-temperature LA MW CVD system to deposit diamond overlays over large areas of LPG-based optical fiber sensors for the first time. The fabricated sensors were used for the label-free detection of proteins. The presence of bovine serum albumin (BSA) bio-layer has been confirmed by the observed change in optical response of the LPG.

2. Experimental and details

A single mode optical fiber (cladding diameter of 125 mm, approx. 20 cm in length) whose polymer coating had been mechanically stripped, and a set of reference samples, i.e. fused silica glass and p-100 Si wafers were prepared. The fabrication procedure of LPGs with a computer-assisted precision arc-discharge apparatus was described in the previous report [22]. At this stage of the experiment, we used the samples of Corning SMF28 fiber to write gratings with a period of $\Lambda = 345$ μm.

The diamond films were grown on the optical fiber using a LA MW CVD system. The size of growth chamber enabled the use of substrates with dimensions of up to 300 × 300 mm. Several NCD films were produced using the following process conditions: gas mixtures containing H_2, CH_4 and CO_2 at various ratios; process pressure 0.1 mbar [21,23,24]; and the total flow rate of gases reaching 150 sccm at the molar ratios of 2.5 and 6% for methane and carbon dioxide, respectively. During the deposition process, the LA MW CVD system was operated in a continuous mode, which resulted in the continuous wave at a maximum power of 1.9 kW (divided over eight antennas) and the growth time of up to 7 h. The temperature of substrate table measured during the procedure was ca. 350 °C. The growth process was preceded by a double immersion of the optical fiber in the diamond suspension, each time for 1 min. In the second step, the fiber was turned around and its other end was dipped. Moreover, the reference quartz slides were seeded in the same seeding media by means of spin-coating [16].

The experimental set-up is schematically shown in Fig. 1. The transmission of LPG samples was measured in the wavelength range from 1150 to 1650 nm using a Yokogawa AQ4305 white light source and Yokogawa AQ6370B optical spectrum analyzer. Bovine serum albumin (BSA) was selected as a model of protein. Firstly, the optical fiber with

induced LPGs was immersed in DI water. Secondly, the sensor structure was dipped twice in the BSA solution and flushed extensively with water. The transmission was monitored at each step of the procedure. BSA is the principal extracellular protein of the circulatory system, and includes most of the total plasma proteins [25]. The chemical sequence of BSA is in 76% identical with human serum albumin (HSA) [26]. Due to the above properties, structural similarities and the low production cost of BSA, HSA is very often replaced by BSA in many laboratories.

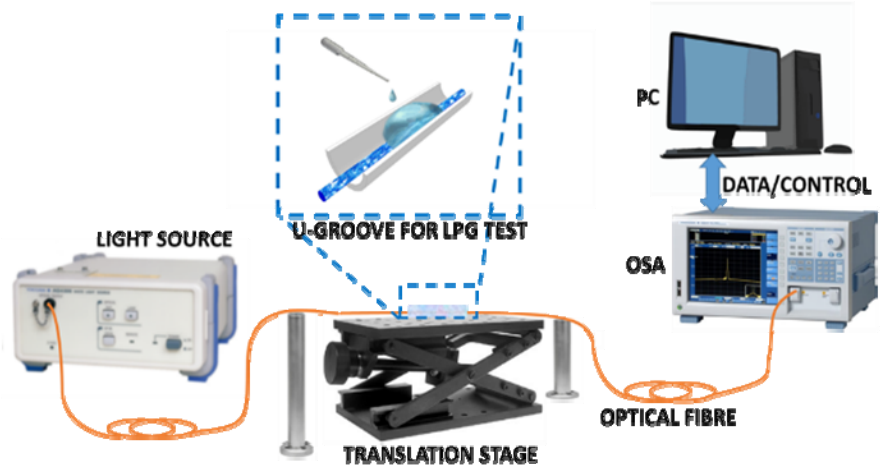

Fig. 1. The experimental set-up.

Scanning Electron Microscope FEI Quanta FEG 250 Scanning Electron Microscope (SEM) using 15kV beam accelerating voltage with SE-ETD detector (secondary electron - Everhart-Thornley detector) working in high vacuum mode (pressure 10^{-4} Pa) was used to observe the structure of the optical fiber surface.

The molecular composition of the films was studied by means of Raman spectroscopy using confocal Raman microscope (Horiba LabRAM ARAMIS, Japan). Spectra were recorded in a range of 200–3500 cm^{-1} with an integration time of 2 s, using a 532 nm diode pumped solid state (DPSS) laser in combination with a 100x objective magnification (NA = 0.95) and 50 µm confocal aperture. The relative sp^3/sp^2 band ratio has been defined as a relation between the Raman band areas of (I) sp^3 diamond lattice line (1332 cm^{-1}), and (II) "G" band assigned to the distorted sp^2 phase (1520-1600 cm^{-1}). The areas of Raman bands were estimated by deconvolution and integration of Raman spectra with the use of OriginLab software (OriginLab Corporation, USA).

Spectroscopic ellipsometry investigation on reference quartz slide was carried out with a Jobin-Yvon UVISEL phase-modulated ellipsometer (HORIBA Jobin-Yvon Inc., Edison, USA). The investigated wavelength region was 250–800 nm with a resolution of less than 0.5 nm. The experiments were carried out at room temperature using an angle of incidence fixed at 60° and the compensator set at 45°. The incidence angle resulted from the Brewster's angle of fused silica substrate. DeltaPsi software (v. 2.4.3) was employed to determine the spectral distributions of refractive index n (λ) and the extinction coefficient k (λ) of the diamond films [27]. The parameters of the TL model were fitted for each of the analyzed films. The NCD surface roughness was estimated by SE using overlayer containing 50% of voids and 50% of NCD film in the optical model. Finally, the assumed optical model was fitted to the experimental data using the nonlinear Levenberg-Marquardt regression method for mean-square error minimization (MSE) [28].

3. Results and discussion

3.1. Surface morphology

Figure 2 displays the SEM micrographs of diamond grown on the optical fiber. The lateral surface of optical fiber is fully and uniformly covered by diamond with no glass deformations or diameter deviations from the telecom standard of 125 μm (Fig. 2(a)). The diamond film is composed of densely packed sharp-edged crystallites with an average size of 0.1 – 0.15 μm, as presented in Fig. 2(b). No significant cracks, defects or impurities were noticed along a 10 cm length of diamond film that had been analyzed.

The grown films exhibit homogeneous morphology without any evident preferential texture. The octahedral and plate-like diamond grains dominate the film because the deposition took place at low temperature, as reported previously in [29]. Both the plates and the octahedral grains are faceted, revealed their crystalline nature. Moreover, the cross-sectional SEM images (not shown here) showed that the optical structure of the fiber core was not modified by the exposure to plasma or process temperature.

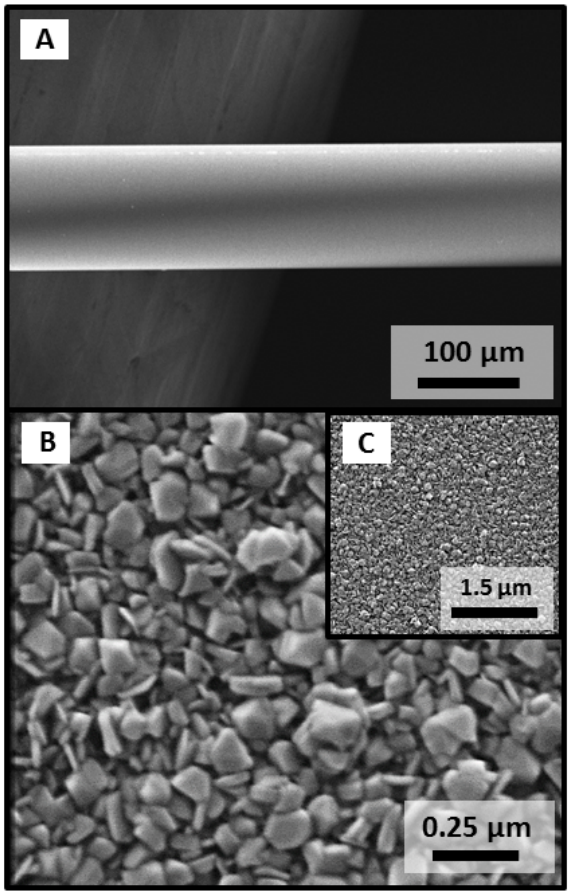

Fig. 2. SEM micrographs of diamond films grown on optical fiber: (A) – a side view of the diamond-coated fiber at a magnification of 250x; (B, C) – enlarged images of the diamond film surface taken at a magnification of 100,000x and 25,000x, respectively.

3.2. Film composition

The Raman spectra of thin diamond film deposited on the optical fiber are presented in Fig. 3. The two main bands observed at 1332 and 1452 cm^{-1} correspond to the diamond phase (sp^3)

and $\delta_{(CH)}$ (transpolyacetylene groups) bands, respectively. The additional weak bands observed at 1562 cm^{-1} are attributable to the graphitic sp^2 carbon phases ("*G*" band), while the band at 1150 cm^{-1} corresponds to the transpolyacetylene-like groups positioned in the intergrain regions [30]. The diamond films grown on optical fibers exhibit spectra similar to those reported for the nanocrystalline diamond materials [31].

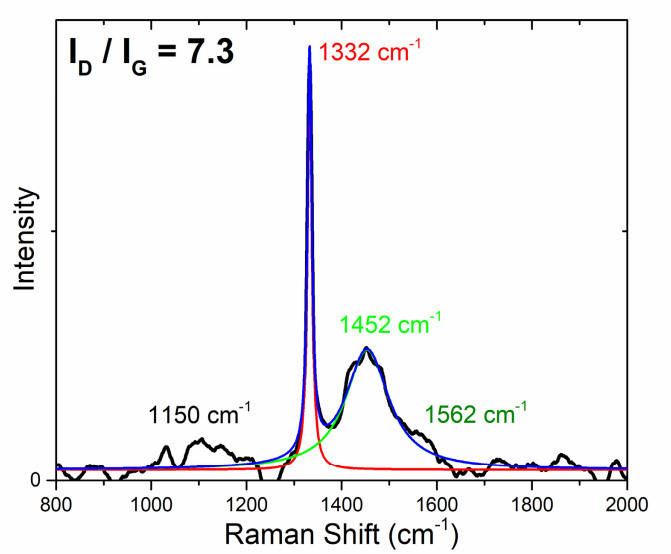

Fig. 3. Normalized Raman spectra of thin diamond film deposited on optical fiber. The peaks were decomposed by using the Lorentzian function.

The peak positions and FWHMs of the diamond peak, $\delta_{(CH)}$ and *G* bands determined from fitting the Lorentzian function are listed in Table 1. The shift of the diamond peak relative to the natural diamond peak located at 1332 cm^{-1} was about 0.8 cm^{-1}, which corresponds to a relatively small tensile residual stress of 0.2 GPa. The full width at half maximum (FWHM) of the diamond peak was in the range that is typical for CVD diamond (10-12 cm^{-1}) in the diamond samples with low amounts of defects.

Table 1. Peak frequencies, bandwidths and relative intensities of bands in the Raman spectra of diamond film deposited on optical fiber.

	band [cm^{-1}]	FWHM [cm^{-1}]
Diamond	1332.8	11.1
$\delta_{(CH)}$	1452.0	102.8
G	1562.5	37.4

The shift of the Raman bands assigned to diamond and the value of bandwidth (FWHM) are mainly attributed to the local stresses at the film/fused silica interface (fiber), which is an effect of non-epitaxial deposition of polycrystalline diamond on an amorphous substrate. In general, the deposited films were characterized by high quality with the sp^3/sp^2 band ratio of 7.3, which is in agreement with previous findings [23].

3.3. Optical properties

Spectroscopic Ellipsometry (SE) investigations were carried out with a phase-modulated ellipsometer to study the optical constants of the deposited diamond films. The diamond film was assumed to be an isotropic, homogeneous material and its dispersion was fitted to the Tauc-Lorentz oscillator (TL) model. This model has been recently used for amorphous semiconductors by Logothetidis et al. [32,33]. Such materials exhibit a peculiarity due to the

presence of two separated contributions of inter-band electronic transition related to sp^2 and sp^3 bonded carbon [34]. Due to the difficulty of taking ellipsometric measurements directly on the curved surface of optical fibers, the measurements were performed on the reference diamond films deposited on quartz slides during the same deposition process. The applied fitting procedure resulted in accurate values of film thickness, film roughness as well as dispersion of refractive index and extinction coefficient.

As a result of SE analysis, the thickness and optical constants, i.e. refractive index n(λ) and extinction coefficient k(λ) were obtained. The changes in the values of *n* and *k* of NCD films are presented in Fig. 4(a). The obtained *n* values were high, ranging from 2.45 to 2.0. Hu et al. [35] reported the values of *n* between 2.16 and 2.08 for the NCD films of 200 nm in thickness. Thus, the deposition of NCD film achieves growth rate of 30 nm · h^{-1}.

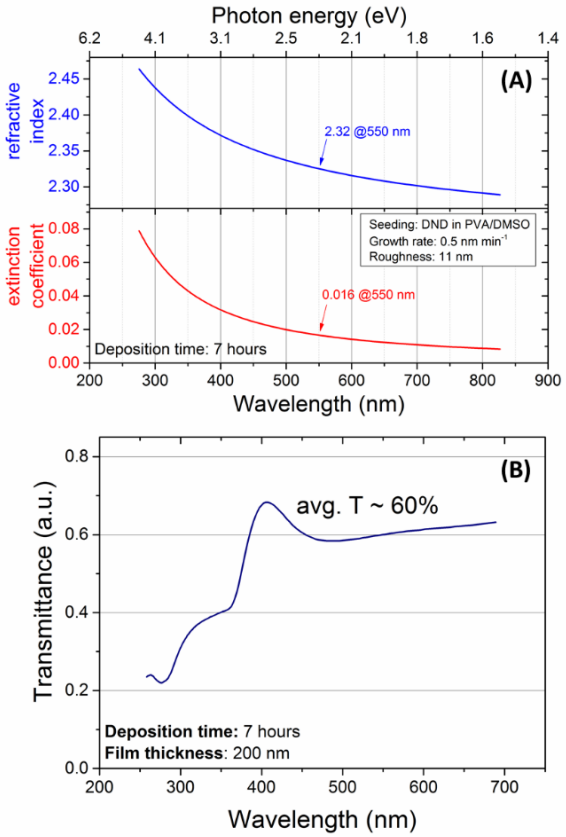

Fig. 4. Dispersion of *n* and *k* (A) and the transmittance (B) of diamond film measured on quartz slide.

The lower *n* value (compared to single crystalline diamond) indicates a lower physical density of the films [36]. The optical constant *k*, corresponding to the optical absorption in the deposited films, was below 0.1 at 550 nm, which indicates low light absorption over the entire length of the optical fiber. The NCD films showed roughness of 11 nm estimated by SE studies showing high agreement with values reported by other groups derived by SE or AFM techniques [37]. The plot of transmittance for the NCD films grown on quartz glass substrates is shown in Fig. 4(b). It can be observed that the transmittance is below 40% in the 300-400 nm range, and it increases to over 60% for the wavelengths above 550 nm. The observed in UV absorption edge originates from fused silica substrate. It is worth noting that NCD film also contribute to that edge adding the absorption attributed to the non-diamond carbon faces

located at nanocrystalline grain boundaries and increasing the subgap density of states [38]. The deposition process was optimized taking into consideration that the obtained NCD will be used in the optical fiber grating devices [39]. It should be mentioned that the observed effects can be partially explained by the denser microcrystalline structure of NCD films deposited directly on quartz slides compared to that of NCD films deposited directly onto the fibers.

Transmission spectra for the LPG sample before and after NCD film deposition are shown Fig. 5. As a result of the deposition process, the resonances shifted in relation to transmission and wavelength. The resonance corresponds to the coupling of the highest order of cladding modes. The coupling affected the resonance peak positioned at (λ_1). After the deposition of NCD overlay, the peak shifted by approx. 15 nm towards shorter wavelengths to the position ($\lambda_{1\text{-}D}$).

The presence of overlay also enhanced the resonance shift in the sample immersed in water. Both these effects prove that the overlay with high n values has been deposited which increased the sensor sensitivity to external RI (n_{ext}) in the RI range close to that of water.

It can be seen that the resonance spectral depth was slightly reduced as a result of deposition, most likely due to the process temperature [40].

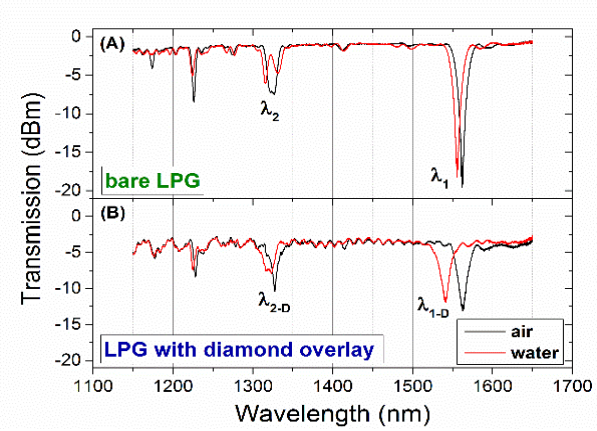

Fig. 5. Comparison of LPG transmission spectra before and after the deposition of diamond overlay for two selected external refractive indices (n_{ext} = 1 and 1.333 RIU).

Next, the biosensing experiment was performed. Because the highest spectral shift occurs for the resonance $\lambda_{1\text{-}D}$ with n_{ext}, i.e. its tracing offers the highest sensitivity, we focused on its observation during this part of the experiment. Figure 6 shows that the immersion in BSA induced a shift of the resonance towards longer wavelengths and the resonance broadening (2nd dip in BSA). After the sample had been washed, the resonance partly returned to its initial position, i.e. it shifted towards shorter wavelengths. However, the observed shift was towards longer wavelengths when referred to the initial spectrum recorded in water (Table 2).

Table 2. Resonance wavelength and its shift at different stages of the experiment.

Stage	wavelength (nm)	shift* (nm)
1. DI water pre-dip	1542.1	-
2. BSA 1st dip	1543.2	1.1
3. BSA 2nd dip	1545.7	2.5
4. Flushed with DI water	1542.9	0.8

* The shift is defined relative to stage 1.

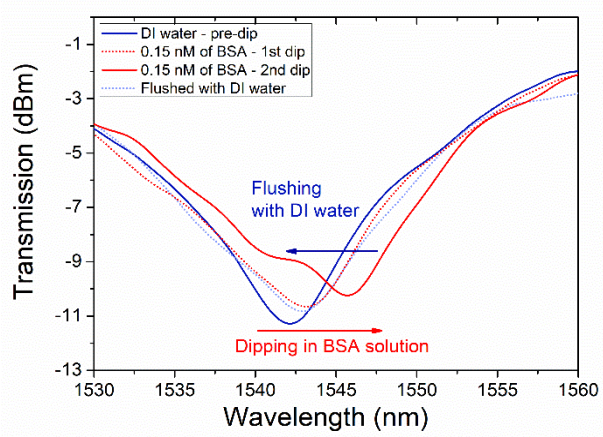

Fig. 6. A response of diamond-coated LPG dipped in 0.15 nM aqueous solution of bovine serum albumin as recorded in the $\lambda_{1\text{-}D}$ wavelength range.

These results indicate that the binding of BSA molecules to the NCD-coated LPG took place. However, the direction of the shift is not in agreement with previously published results on the formation of thin biological film on the LPG surface [41]. It should be emphasized here that the previously shown effects were discussed for uniformly deposited overlays where the coupling of symmetrical cladding modes had taken place. In the case of NCD film, the overlay distribution around the fiber may not be uniform, thus the coupling of asymmetrical modes must be considered. We discussed the effect of the response to n_{ext} in our previous work in which the LPGs were non-uniformly coated with diamond-like carbon overlays [42].

In such case, the resonance splits into multiple resonances with increasing n_{ext}. Typically, only the resonance formed at shorter wavelengths experiences blue shift with increasing n_{ext}, while the others preserve their spectral position or even shift slightly towards longer wavelengths. It is likely that such an effect also occurred in this experiment. The split into two resonances is clearly visible for the 2nd dip in BSA (Fig. 6), which corresponds to the highest n_{ext} and the thickest bio-layer formed on the NCD surface. Nevertheless, the results after immersion in BSA indicate some protein attachment to the NCD-coated LPG-sensor. After the attachment of BSA, flushing with DI water partly removed the proteins that could not bound effectively to the NCD surface. The response after flushing was similar to that after the first dipping, indicating that BSA had formed a bio-layer at the NCD surface.

The resulting sensitivity of presented NCD-coated LPG is able to achieve BSA detection at concentrations as low as 0.15 nM. Similar limit of detection could be achieved for pathogen or cancer originated proteins. Most of the optical biosensing techniques offer similar or worse limits of detection using much more complicated design. For example, protein detection by optical shift of a resonant microcavity showed saturation for BSA concentrations at 20 nM [43], and an in-fiber Mach-Zehnder interferometric biosensor had a detection limit of 3.5×10^{-5} RIU [41]. A surface plasmon resonant optical fber sensors showed detection of Staphylococcal enterotoxin B at the sensor refractive index sensitivity of about 3150 nm per RIU [44], and the lowest limit of detection (LOD) of 100 fg/mL (3 fM) for free prostate specific antigen [45]. Different plasmonic approach, a surface-enhanced Raman spectroscopy was shown utilizing HSA (Human Serum Albumin) with LOD of four main drug classes in the range of 90-400 ng/ml [46]. Both approaches offer lower LODs, but gold films are not-resistant like diamond to highly reactive, ion rich human body fluids.

4. Conclusion

In this work, we applied a LA MW CVD method to grow the NCD films on temperature-sensitive optical fiber devices, such as LPGs. The parameters of the proposed process have been optimized to obtain high quality coating grown at a low temperature. A high refractive index of 2.32 and an extinction coefficient of 0.016 at $\lambda = 550$ nm were achieved. Since LPGs are known for their high sensitivity to changes in the optical properties of an external medium, the deposition of the film was confirmed by a significant shift of resonances in the LPG transmission spectrum. Moreover, we have shown that the NCD-coated LPG structure is a promising platform for the label-free bio-sensing. We have demonstrated that the developed biosensor is capable of detecting the formation of BSA-based bio-layer. Despite the non-uniform NCD thickness around the fiber, the NCD-coated LPG clearly responded to the attachment of proteins. Further chemical functionalization of NCD coating may allow for the development of a robust biosensor suitable for the detection of specific bio-molecules.

Funding

This work was supported by the research grant NATO SPS G5147 and by Polish National Science Centre (NCN) under the Grants No. 2014/14/M/ST5/00715, 2014/14/E/ST7/00104 and 2016/21/B/ST7/01430. The DS funds of Faculty of Electronics, Telecommunications and Informatics of the Gdansk University of Technology are also acknowledged.

Acknowledgments

The LA MW CVD apparatus was obtained through financial support of the Hercules Foundation.